COMMUNICATION

Check for updates

Circularly polarized luminescent organogels based on fluorescence resonance energy transfer in an achiral polymer system†

Yinglong Bao,‡[a] Gong Zhang,‡*[a] Nianwei Wang,[a] Menghan Pan[a] and Wei Zhang [ID] *[ab]

Here we develop circularly polarized luminescent organogels through supramolecular co-assembly of an achiral polymer with guest molecules. Appropriate matching and stacking enable circularly polarized fluorescence resonance energy transfer in the organogels and a wavelength shift and amplified g_{lum} value are further achieved. The current strategy provides a new way to construct CPL-active soft materials.

Chirality is ubiquitous in nature and living systems.[1–3] Many chirality-related studies have been intensively carried out to investigate the origin of chirality and fabricate chiral functional materials.[4–7] Chirality information can be divided into different absorption (ground state) and emission (excited state) of left (L)- and right (R)-handed circularly polarized light, respectively.[8] Accordingly, exploring circularly polarized luminescence (CPL) not only facilitates understanding of the nature of chirality in the excited state but also helps us to develop novel chiroptical materials.[9] In recent years, CPL-active materials have attracted tremendous attention because of their significant application prospects in three-dimensional displays,[10] information storage,[11] smart sensors,[12] and asymmetric photochemical synthesis.[13–15] Many chiral systems including metal complexes,[16–18] chiral liquid crystals,[19–21] helical peptide arrays,[22] helical polymers,[23–28] and chiral supramolecular assemblies[29–32] have been extensively investigated. In general, CPL-active materials can be fabricated by encapsulating achiral luminescent organic molecules into chiral matrixes.[32–34] Alternatively, fluorescent organic chromophores

themselves with a single chiral property (such as planar chirality) or covalently linked to chiral groups can also be highly CPL-active materials.[17,35–37] However, the fabrication of chiral polymeric gel materials with controlled CPL emission is rarely investigated. The facile modulation of wavelength, CPL handedness, and luminescence dissymmetry factor (g_{lum}) enhancement in gel systems is very challenging.

As one kind of special aggregated material, a polymer gel is a three-dimensional network of interlaced polymer chains that trap many solvent molecules.[38] The solvent usually includes water or organic solvent molecules, which correspond to hydrogels or organogels, respectively. Gel materials have many unique advantages, including flexibility and easy processing capability, which make them excellent candidates for flexible electronics and sensing devices.[38–40] Although several groups have reported CPL-active gels,[41–43] chiral gelators (*i.e.*, amino-acid- and sugar-based derivatives) generally need tedious synthetic procedures. Meanwhile, the handedness and wavelength of CPL are hard to regulate since it usually needs sophisticated chemical synthesis of the gelator with opposite chirality. Therefore, the fabrication of CPL-active gels with flexibly adjustable handedness, wavelength and high g_{lum} values formed by a changeless gelator remains a challenge.

Herein, according to our previous study on the gelation process of an achiral polymer poly(9,9-di-*n*-octylfluorene) (PF8) in chiral *R/S*-limonene solution,[44] we prepared CPL-active organogels with blue CPL emission and moderate g_{lum} values (Fig. 1a). When the appropriate guest molecule coumarin6 (Cou6) co-assembled with PF8 and limonene (Fig. S1, ESI†), a new chiral organogel (PF8@Cou6) with green emission was formed due to circularly polarized fluorescence resonance energy transfer (*C*-FRET) (Fig. 1b). The supramolecular chirality could be successfully transferred to Cou6 molecules. Moreover, the as-prepared PF8@Cou6 organogels exhibited higher g_{lum} ($\sim 10^{-2}$) than the former. The *C*-FRET process not only enabled a wavelength shift but was also crucial for the enhancement of the dissymmetry factor. Compared to the traditional method of chemical synthesis of gelators with opposite

[a] State and Local Joint Engineering Laboratory for Novel Functional Polymeric Materials, Jiangsu Engineering Laboratory of Novel Functional Polymeric Materials, Suzhou Key Laboratory of Macromolecular Design and Precision Synthesis, College of Chemistry, Chemical Engineering and Materials Science, Soochow University, Suzhou Industrial Park, Suzhou 215123, P. R. China. E-mail: gzhang177@suda.edu.cn, weizhang@suda.edu.cn

[b] School of Chemical and Environmental Engineering, Anhui Polytechnic University, Wuhu 241000, P. R. China

† Electronic supplementary information (ESI) available. See DOI: https://doi.org/10.1039/d2tc05101j
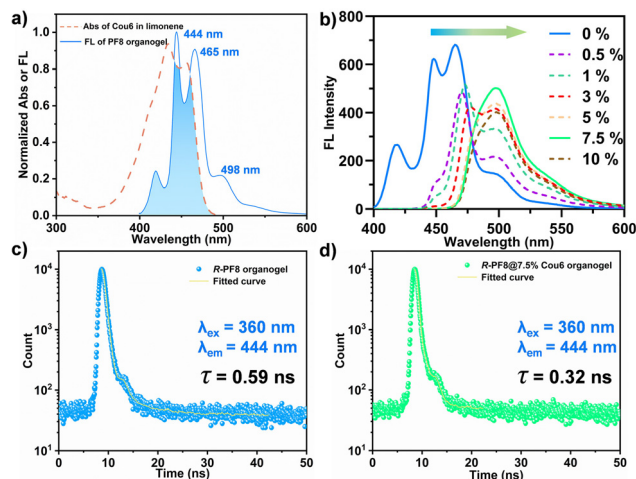
‡ These authors contributed equally to this work.
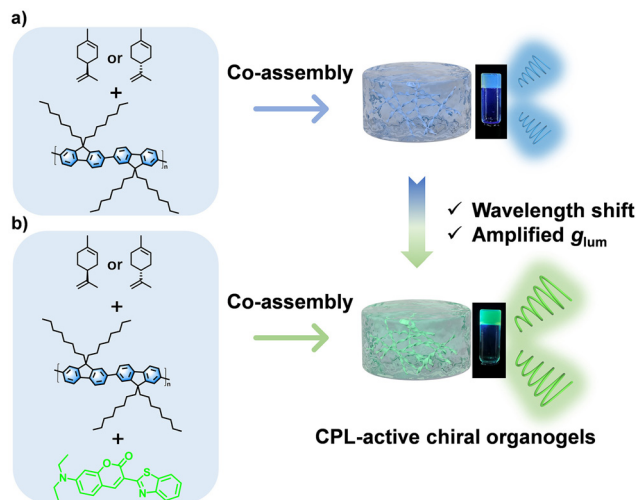
Fig. 1 Schematic illustration of the two chiral co-assembly processes: (a) co-assembly of *R/S*-limonene and PF8 into blue CPL-active chiral organogels and (b) co-assembly of *R/S*-limonene, PF8 and Cou6 into green CPL-active chiral organogels with higher g_{lum} values.

Fig. 2 (a) The UV-vis spectra of a Cou6 solution of and fluorescence spectra (FL) of PF8 organogels; (b) the FL spectra of PF8@Cou6 organogels with different molar ratios of Cou6 (7.5% represents PF8 repeating units and Cou6 in a molar ratio of 100 to 7.5). λ_{ex} = 360 nm. (c) Fluorescence decay and fitted curves of the *R*-PF8 organogel and (d) *R*-PF8@Cou6 organogel.

chirality, the handedness of CPL could be facilely controlled by the chirality of the solvent limonene. These soft gel materials with chiroptical features exhibit bright application prospects in advanced information encryption, especially with the rapid development of smart wearable devices.

PF8 polymer with high molecular weight (M_n = 32 300 g mol^{-1}, $Đ$ = 3.26) was synthesized by the Suzuki polycondensation reaction (Fig. S1–S3, ESI†). The co-assembly experiments were carried out at −20 °C. After incubation for five hours without any disturbance, light yellow organogels were observed under ambient light. The formation of gels was initially confirmed by the inverted tube experiment (Fig. S4, ESI†). A previous study indicated that one of the necessary conditions for the FRET process was the overlap of the emission of the donor and absorbance of the acceptor. Hence, as shown in Fig. 2a, the UV-vis spectra of Cou6 solution and fluorescence spectra (FL) of PF8 organogels were obtained. Three typical peaks in the FL spectra of the PF8 organogels at 444, 465 and 498 nm confirmed the formation of a thermodynamically metastable β-phase, which was a highly delocalized π-electron structure.[44] This structure promoted its co-assembly with planar conjugated molecules. The blue area indicated the good overlap of the emission band of PF8 and the absorbance band of Cou6, which was responsible for FRET. By gradually increasing the molar ratio of Cou6 from 0% to 7.5%, the characteristic emission of PF8 at 465 nm decreased and the emission of Cou6 at 498 nm increased, indicating an obvious intermolecular energy transfer (Fig. 2b). However, upon further increasing the content of Cou6 to 10%, the intensity at 498 nm dropped, which may be attributed to the aggregation-caused quenching (ACQ) effect (Fig. S5, ESI†). The energy transfer efficiency reached 97.55% at a molar ratio of 7.5%. The FRET efficiency was distance-dependent. The high energy transfer efficiency also indicated the suitable stacking structure of the PF8 main chains and Cou6. We performed fluorescence decay measurements at 444 nm (characteristic emission peak of the PF8 organogels) to further demonstrate the *C*-FRET process

(Fig. 2c and d). In the absence of the acceptor Cou6, the *R*-PF8 organogel exhibited an average lifetime τ of 0.59 ns at 444 nm (Fig. 2c). However, when 7.5% Cou6 was added into the system, PF8 exhibited the average lifetime τ of 0.32 ns at 444 nm (Fig. 2d), which was lower than that of the PF8 organogel. This result further indicated that efficient energy transfer occurred in the PF8@Cou6 organogels. The fitted parameters of the fluorescence lifetimes of the two organogels at 444 nm excited at 360 nm are given in Table S1 (ESI†). The inverted tube experiment indicated that the co-assembled organogels can be formed with the molar ratios of Cou6 from 0% to 10% (Fig. S4, ESI†). The absolute quantum yields (QYs) of the *R*-PF8 and *R*-PF8@7.5% Cou6 organogels were 68.51% and 37.25%, respectively (Fig. S6, ESI†).

The morphology and mechanical properties of these organogels were measured. The typical high-resolution transmission electron microscopy (HRTEM) and atomic force microscopy (AFM) images of *R/S*-PF8 and *R/S*-PF8@Cou6 are given in Fig. 3a and b and Fig. S7–S9 (ESI†). As shown in Fig. 3a and b and Fig. S7 (ESI†), well-defined nanofibers were observed in the *S*-PF8 and *S*-PF8@Cou6 organogels. The average diameter of the nanofibers of *S*-PF8 was statistically measured to be 34.1 nm. However, for *S*-PF8@Cou6, the diameter increased to 42.8 nm, which may be attributed to the further stacking of PF8 and Cou6. The slight left-handed helical structure (*M*-helix) was also observed in the edge of the nanofibers. In Fig. 3a and b, the typical nanofibers in red circles show an obvious change of screw pitch. Compared to PF8 organogels, nanofibers of PF8@Cou6 became thicker and showed higher degree of wrinkling (lower screw pitch). Similar results were obtained in Fig. S8 (ESI†) for *R*-PF8 and *R*-PF8@Cou6 organogels. An opposite helical structure (*P*-helix) was achieved. The diameters of the *R*-PF8 and *R*-PF8@Cou6 organogels were measured to be 23.6 and 25.6 nm, respectively. Interlaced and uniform nanofibers were also observed in the *R/S*-PF8 and *R/S*-PF8@Cou6 organogels in the AFM images (Fig. S9, ESI†),
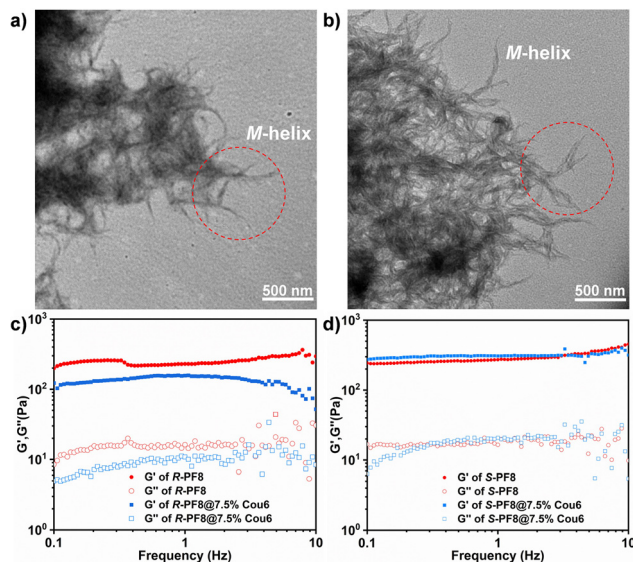
Fig. 3 The HRTEM images of *S*-PF8 organogel (a) and *S*-PF8@7.5% Cou6 organogel (b) and the dynamic frequency sweep test of *R*-PF8 and *R*-PF8@7.5% Cou6 organogels (c) and *S*-PF8 and *S*-PF8@7.5% Cou6 organogels (d) at a strain of 0.1% and at 25 °C.

Fig. 4 The CD spectra of *R*/*S*-PF8 (a) and *R*/*S*-PF8@7.5% Cou6 organogels (b); CPL spectra (c) and g_{lum} values (d) of *R*/*S*-PF8 and *R*/*S*-PF8@7.5% Cou6 organogels. The insets in (c) show the digital images of the organogels under UV irradiation.

which were consistent with the TEM measurements. Dynamic and static rheological measurements were performed to study the mechanical properties of the organogels. As shown in Fig. 3c and d, a dynamic frequency sweep test of *R*/*S*-PF8 and *R*/*S*-PF8@ 7.5% Cou6 was performed. The storage modulus G' of all the as-prepared samples was higher than the corresponding loss modulus G'', indicative of the formation of stable viscoelastic organogels. For *R*-PF8 and *R*-PF8@7.5% Cou6 organogels, *R*-PF8 showed higher G' and G'' than *R*-PF8@7.5% Cou6 organogels, suggesting that the addition of Cou6 would slightly reduce the mechanical strength of the organogels. This result can be confirmed by AFM experiments. Thicker and relatively loose porous nanofibers were formed in *R*-PF8@7.5% Cou6 organogels, which was unfavourable for enhancement of the mechanical strength. However, for *S*-PF8 and *S*-PF8@7.5% Cou6 organogels, the G' and G'' were almost equal. These results indicated that the chiral structure may slightly affect the mechanical properties of the gels.[45] The complex viscosity and frequency curves were consistent with the frequency sweep test (Fig. S10, ESI†). Static rheological measurements demonstrated that these organogels were very stable under the strain of 0.1% at 25 °C, although the preparation process was carried out at low temperatures (Fig. S11, ESI†). It should be noted that the gel structure can be maintained over one year.

The chiroptical feature of these organogels was investigated by circular dichroism (CD) and CPL measurements. As shown in Fig. 4a, the *R*-PF8 and *S*-PF8 showed mirrored CD signals, indicating the chirality transfer from *R*/*S*-limonene to PF8 ensembles. The *R*-PF8 organogel exhibited positive cotton effects at 407 nm and 436 nm and a negative cotton effect at 446 nm. The peak at 446 nm was attributed to the helical stacking of the PF8 main chain (β-phase). The *S*-PF8 organogel exhibited contrary experimental results. When Cou6 molecules were added into PF8 and limonene solution, the co-assembled
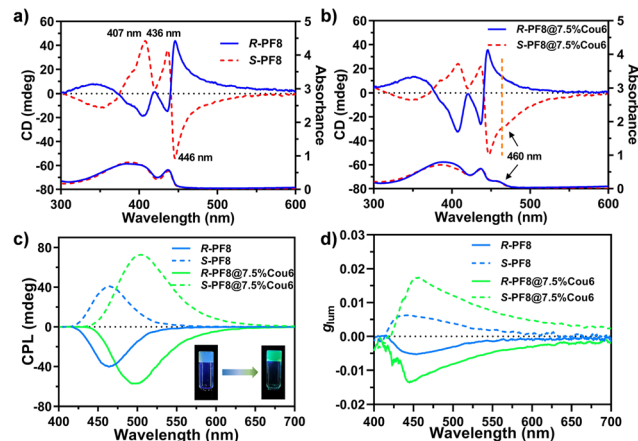
organogels showed similar CD signals, indicating that the incorporation of Cou6 molecules would not damage the chiral structure of PF8 (Fig. 4b). Moreover, the signal at 460 nm (orange line), corresponding to the absorbance of Cou6 suggested the successful chirality transfer from PF8 to Cou6 molecules. The chirality transfer in the ground state laid the foundation for subsequent *C*-FRET (chirality transfer in excited states). The CPL spectra of the organogels are presented in Fig. 4c. The mirrored CPL signals were measured in the *R*/*S*-PF8 organogels and *R*/*S*-PF8@7.5% Cou6, respectively. The *R*/*S*-PF8 organogels exhibited intensive CPL signals at 464 nm, which was consistent with the FL spectra in Fig. 2a. After the incorporation of Cou6 molecules, a redshift of the CPL wavelength occurred, indicative of chirality and energy transfer. The CPL maximum of *R*/*S*-PF8@7.5% Cou6 red shifted to 498 nm. The digital images (insets in Fig. 4c) also clearly demonstrated the wavelength shift from blue to green fluorescence under UV irradiation. The experimental results were consistent with the DC curves in Fig. S12 (ESI†). The g_{lum} curves in Fig. 4d demonstrated the amplification of the g_{lum} values of the *R*/*S*-PF8@7.5% Cou6 organogels compared to those of *R*/*S*-PF8. The g_{lum} values of *R*/*S*-PF8 at 464 nm were -5.0×10^{-3} and 5.4×10^{-3}, respectively. The g_{lum} values of the *R*/*S*-PF8@7.5% Cou6 organogels at 498 nm increased to -8.4×10^{-3} and 1.2×10^{-2}, respectively. For the *S*-PF8@7.5% Cou6 organogels, a more than two-fold amplification was achieved. These results indicated that the incorporation of Cou6 could not only arouse the wavelength shift due to *C*-FRET but also facilitate the enhancement of the g_{lum} values. More importantly, the gel structure with good mechanical properties could be maintained at the same time, as described above. The speculated reason for the enhancement of the g_{lum} values could be attributed to the following two aspects: (1) the change of morphology caused by the higher degree of helical structure (lower screw pitch) after co-assembly with Cou6, demonstrated by HRTEM and AFM images in Fig. 3a and b and Fig. S7–S9 (ESI†); (2) the former CPL harvested by the Cou6 molecules, other than regularly unpolarized light excitation.[43] In addition, the heat treatment experiments further proved the

This journal is © The Royal Society of Chemistry 2023

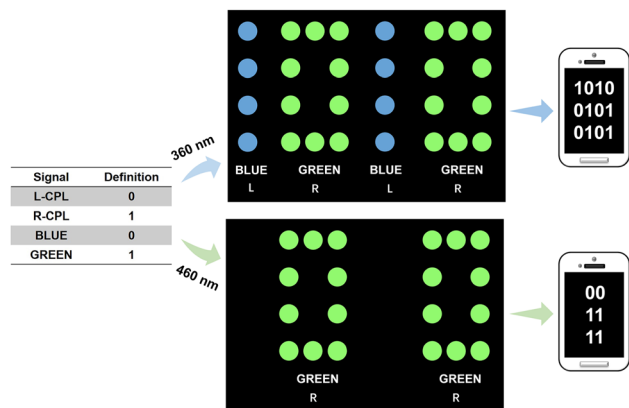*J. Mater. Chem. C*, 2023, **11**, 2475–2479 | **2477**

Fig. 5 The designed multiple information encryption of binary code formed by the as-prepared organogels with different CPL wavelengths and handedness.

relationship between the gel structure and energy transfer and CPL performance (Fig. S13–S15, ESI†). Instead of Cou6 with 3-amino coumarin (3-Cou) in the assembly system, a similar experiment was conducted (Fig. S17a, ESI†). Although 3-Cou molecules have a similar structure to Cou6 (Fig. S1, ESI†), the emission overlap of PF8 and absorbance of Cou6 was almost nonexistent (Fig. S16, ESI†). It can be predicted that FRET from PF8 to 3-Cou could not occur. Although the co-assembled PF8@3-Cou organogels could be formed (insets in Fig. S17b, ESI†), the CPL and DC curves demonstrated that only PF8 signals could be detected (Fig. S17b, ESI†). Moreover, a lower g_{lum} value was obtained (Fig. S17c, ESI†), which may be attributed to the inappropriate stacking structure of co-assembly. These results demonstrated that the introduction of unsuitable guest molecules not only failed to achieve the wavelength shift but also led to the degradation of the CPL performance.

CPL exhibited left- or right-handed polarized light, which could be regarded as part of a high-level visual perception for affording one more dimension of information, compared to traditional fluorescence. Solid-phase information encryption was more practical than that of liquid phase.[46] As special aggregated materials, gels have properties similar to those of solids and have special advantages in the fabrication of flexible smart materials. Therefore, we designed a new multiple information encryption system based on the as-prepared organogels with different wavelengths and handedness (Fig. 5). First, the definition of L-CPL and R-CPL was given as 0 and 1, respectively. Second, the definition of blue and green emission was given values of 0 and 1, respectively. We used a four-digit system as an example. When the system was exposed to UV irradiation in dark surroundings, a multiple binary code (1010, 0101, and 0101) could be identified. This binary code could be further decrypted into concrete information by software. If another excitation light (460 nm only for Cou6 excitation) was applied, completely different information (00, 11, and 11) could be identified. Accordingly, CPL-active materials are candidates for the design of high-level information encryption, especially for gel materials.

In summary, we have fabricated supramolecular organogels with blue and green CPL emission based on an achiral polymer

PF8. The wavelength can be regulated by *C*-FRET through co-assembly with the appropriate guest molecule Cou6 and a more than two-fold amplification of g_{lum} values is achieved. The handedness of the CPL signals can be facilely regulated by the chirality of the chiral solvent limonene. Organogels with controlled wavelengths and handedness exhibit significant application prospects in information encryption. This work provides a new way to construct CPL-active soft functional materials.

Conflicts of interest

There are no conflicts of interest.

Acknowledgements

Notes and references

1 M. Liu, L. Zhang and T. Wang, *Chem. Rev.*, 2015, **115**, 7304–7397.
2 E. Yashima, K. Maeda, H. Iida, Y. Furusho and K. Nagai, *Chem. Rev.*, 2009, **109**, 6102–6211.
3 A. Cecconello, L. V. Besteiro, A. O. Govorov and I. Willner, *Nat. Rev. Mater.*, 2017, **2**, 1–19.
4 L. Yin, M. Liu, H. Ma, X. Cheng, T. Miao, W. Zhang and X. Zhu, *Sci. China: Chem.*, 2021, **64**, 2105–2110.
5 X. Cheng, T. Miao, L. Yin, Y. Ji, Y. Li, Z. Zhang, W. Zhang and X. Zhu, *Angew. Chem., Int. Ed.*, 2020, **59**, 9669–9677.
6 G. Zhang, Y. Liang, Y. Wang, Q. Li, W. Qi, W. Zhang, R. Su and Z. He, *ACS Nano*, 2022, **16**, 6866–6877.
7 H.-E. Lee, H.-Y. Ahn, J. Mun, Y. Y. Lee, M. Kim, N. H. Cho, K. Chang, W. S. Kim, J. Rho and K. T. Nam, *Nature*, 2018, **556**, 360–365.
8 T. Zhao, J. Han, P. Duan and M. Liu, *Acc. Chem. Res.*, 2020, **53**, 1279–1292.
9 C. Zhang, S. Li, X. Y. Dong and S. Q. Zang, *Aggregate*, 2021, **2**, e48.
10 Y. Yang, R. C. da Costa, D. M. Smilgies, A. J. Campbell and M. J. Fuchter, *Adv. Mater.*, 2013, **25**, 2624–2628.
11 Y. Wu, C. Yan, X. S. Li, L. H. You, Z. Q. Yu, X. Wu, Z. Zheng, G. Liu, Z. Guo, H. Tian and W. H. Zhu, *Angew. Chem., Int. Ed.*, 2021, **60**, 24549–24557.
12 F. Song, G. Wei, X. Jiang, F. Li, C. Zhu and Y. Cheng, *Chem. Commun.*, 2013, **49**, 5772–5774.
13 L. Wang, L. Yin, W. Zhang, X. Zhu and M. Fujiki, *J. Am. Chem. Soc.*, 2017, **139**, 13218–13226.
14 L. Xu, X. Wang, W. Wang, M. Sun, W. J. Choi, J.-Y. Kim, C. Hao, S. Li, A. Qu and M. Lu, *Nature*, 2022, **601**, 366–373.

2478 | *J. Mater. Chem. C*, 2023, **11**, 2475–2479

This journal is © The Royal Society of Chemistry 2023

15 D. Han, X. Yang, J. Han, J. Zhou, T. Jiao and P. Duan, *Nat. Commun.*, 2020, **11**, 5659.

16 R. Zhai, Y. Xiao, Z. Gu and J. Zhang, *Nano Res.*, 2021, **15**, 1102–1108.

17 S. G. Kang, K. Y. Kim, Y. Cho, D. Y. Jeong, J. H. Lee, T. Nishimura, S. S. Lee, S. K. Kwak, Y. You and J. H. Jung, *Angew. Chem., Int. Ed.*, 2022, **61**, e202207310.

18 J. G. Yang, K. Li, J. Wang, S. Sun, W. Chi, C. Wang, X. Chang, C. Zou, W. P. To, M. D. Li, X. Liu, W. Lu, H. X. Zhang, C. M. Che and Y. Chen, *Angew. Chem., Int. Ed.*, 2020, **59**, 6915–6922.

19 J. He, K. Bian, N. Li and G. Piao, *J. Mater. Chem. C*, 2019, **7**, 9278–9283.

20 M. Xu, C. Ma, J. Zhou, Y. Liu, X. Wu, S. Luo, W. Li, H. Yu, Y. Wang, Z. Chen, J. Li and S. Liu, *J. Mater. Chem. C*, 2019, **7**, 13794–13802.

21 P. Lu, Y. Chen, Z. Chen, Y. Yuan and H. Zhang, *J. Mater. Chem. C*, 2021, **9**, 6589–6596.

22 Q. Li, J. Zhang, Y. Wang, G. Zhang, W. Qi, S. You, R. Su and Z. He, *Nano Lett.*, 2021, **21**, 6406–6415.

23 X. Gao, J. Wang, K. Yang, B. Zhao and J. Deng, *Chem. Mater.*, 2022, **34**, 6116–6128.

24 X.-X. Cheng, T.-F. Miao, L. Yin, W. Zhang and X.-L. Zhu, *Chin. J. Polym. Sci.*, 2021, **39**, 1357–1375.

25 G. Zhang, X. Cheng, Y. Wang and W. Zhang, *Aggregate*, 2022, **262**, DOI: 10.1002/agt1002.1262.

26 Z. Geng, Y. Cheng, Y. Zhang, Y. Zhang and Y. Quan, *Angew. Chem., Int. Ed.*, 2022, **61**, e202202718.

27 Q. Li, J. Yuan, H. Liang, F. Zheng, X. Lu, C. Yu and Q. Lu, *ACS Nano*, 2020, **14**, 8939–8948.

28 N. Lu, X. Gao, M. Pan, B. Zhao and J. Deng, *Macromolecules*, 2020, **53**, 8041–8049.

29 J. C. Y. Ng, H. Li, Q. Yuan, J. Liu, C. Liu, X. Fan, B. S. Li and B. Z. Tang, *J. Mater. Chem. C*, 2014, **2**, 4615–4621.

30 D. Niu, Y. Jiang, L. Ji, G. Ouyang and M. Liu, *Angew. Chem., Int. Ed.*, 2019, **58**, 5946–5950.

31 L. Ji, Y. Zhao, M. Tao, H. Wang, D. Niu, G. Ouyang, A. Xia and M. Liu, *ACS Nano*, 2020, **14**, 2373–2384.

32 Y. X. Yuan, J. H. Jia, Y. P. Song, F. Y. Ye, Y. S. Zheng and S. Q. Zang, *J. Am. Chem. Soc.*, 2022, **144**, 5389–5399.

33 J. Han, J. You, X. Li, P. Duan and M. Liu, *Adv. Mater.*, 2017, **29**, 1606503.

34 X. Yang, X. Jin, L. Zhou, P. Duan, Y. Fan and Y. Wang, *Angew. Chem., Int. Ed.*, 2022, **61**, e202115600.

35 R. Liu, Z. Feng, C. Cheng, H. Li, J. Liu, J. Wei and Z. Yang, *J. Am. Chem. Soc.*, 2022, **144**, 2333–2342.

36 H. Li, J. Cheng, H. Deng, E. Zhao, B. Shen, J. W. Y. Lam, K. S. Wong, H. Wu, B. S. Li and B. Z. Tang, *J. Mater. Chem. C*, 2015, **3**, 2399–2404.

37 J. Li, P. Li, M. Fan, X. Zheng, J. Guan and M. Yin, *Angew. Chem., Int. Ed.*, 2022, **61**, e202202532.

38 A. H. Williams, S. Roh, A. R. Jacob, S. D. Stoyanov, L. Hsiao and O. D. Velev, *Nat. Commun.*, 2021, **12**, 2834.

39 Y. Shi, O. Ilic, H. A. Atwater and J. R. Greer, *Nat. Commun.*, 2021, **12**, 2797.

40 B. Ding, P. Zeng, Z. Huang, L. Dai, T. Lan, H. Xu, Y. Pan, Y. Luo, Q. Yu, H. M. Cheng and B. Liu, *Nat. Commun.*, 2022, **13**, 1212.

41 S. Du, X. Zhu, L. Zhang and M. Liu, *ACS Appl. Mater. Interfaces*, 2021, **13**, 15501–15508.

42 R. Cao, X. Yang, Y. Wang and Y. Xiao, *Nano Res.*, 2023, **16**, 1459–1464.

43 L. Ji, Y. Sang, G. Ouyang, D. Yang, P. Duan, Y. Jiang and M. Liu, *Angew. Chem., Int. Ed.*, 2019, **58**, 844–848.

44 Y. Zhao, N. A. Abdul Rahim, Y. Xia, M. Fujiki, B. Song, Z. Zhang, W. Zhang and X. Zhu, *Macromolecules*, 2016, **49**, 3214–3221.

45 G. Zhang, L. Zhang, H. Rao, Y. Wang, Q. Li, W. Qi, X. Yang, R. Su and Z. He, *J. Colloid Interface Sci.*, 2020, **577**, 388–396.

46 Q. Wang, B. Lin, M. Chen, C. Zhao, H. Tian and D.-H. Qu, *Nat. Commun.*, 2022, **13**, 4185.

This journal is © The Royal Society of Chemistry 2023

J. Mater. Chem. C, 2023, **11**, 2475–2479 | **2479**